Surface structures and crystal morphologies of $LiFePO_4$: relevance to electrochemical behaviour†

Craig A. J. Fisher and M. Saiful Islam*

Received 16th October 2007, Accepted 3rd January 2008
First published as an Advance Article on the web 31st January 2008
DOI: 10.1039/b715935h

Advanced simulation techniques are used to provide atomic-scale insight into the surface structures and crystal morphologies of the lithium battery cathode material $LiFePO_4$. Relaxed surface structures and energies are reported for 19 low index planes. The calculated equilibrium morphology takes on a rounded, isometric appearance, with {010}, {201}, {011}, and {100} faces prominent. Almost all of the low energy surfaces are lithium-deficient relative to the bulk lattice, requiring Li vacancies at the surface. The calculated growth morphology exhibits the {010}, {100} and {101} faces, with an elongated hexagonal prism-like shape; this morphology is more consistent with experimentally observed $LiFePO_4$ particles. The exposure of the (010) surface in our calculated equilibrium and growth morphologies is significant since it is normal to the most facile pathway for lithium ion conduction (along the [010] channel), and hence important for the reversible insertion/de-insertion of lithium ions. SEM images of plate-like crystallites from hydrothermal synthesis are also simulated by our methods, and exhibit large (010) faces.

1. Introduction

In the field of lithium battery research, there is tremendous activity devoted to finding alternatives to cobalt-oxide-based cathodes, particularly for potential use in large-scale applications (such as hybrid electric vehicles).[1] The olivine-structured orthophosphate $LiFePO_4$ has become a highly promising cathode material for use in lithium ion batteries because of its high operating voltage (~3.5 V *vs.* Li/Li^+) and large theoretical gravimetric capacity (~170 mAh g^{-1}), as well as its low cost, non-toxicity and safety advantages.[2–5] One impediment to the wider use of $LiFePO_4$, however, is its low intrinsic conductivity.[6,7] Various approaches have been used to overcome this obstacle, such as preparation of $LiFePO_4$–carbon conductive composites,[4,8–11] formation of metal phosphide networks,[12] addition of supervalent cations[13] and reduction of particle size.[14–18]

The formation of $LiFePO_4$ particles of sub-micron or nanometre size is thought to enhance electrochemical performance by reducing the transport path lengths of lithium ions and electrons. In addition, decreasing the crystallite size is important for the electrode–electrolyte interface, and may also reduce the mechanical lattice strain upon lithium (de)insertion.[14,18] A range of synthesis techniques have been used, *e.g.*, solid-state reaction[2,19] and hydrothermal methods,[14,15,20,21] leading to a variety of particle morphologies and size distributions. Studies of the surface chemistry of these systems have been carried out, for example, using Mössbauer and X-ray photoelectron spectroscopy,[16,22,23] and electron microscopy.[11,20]

It is clear that morphological control of nanocrystalline materials is becoming increasingly important, as many of the properties are highly shape and size dependent.[15,17] Given the importance of surface structure and (nano)particle morphology on the properties of $LiFePO_4$, knowledge of these features on the atomic level would provide valuable information for understanding electrochemical mechanisms. The variety of synthesis techniques, however, makes it difficult to extract such fundamental detail or identify distinct surface planes by experiment alone. We have therefore carried out a computer simulation study using well-established atomistic methods to examine surface structures and crystal morphologies of $LiFePO_4$. Such methods are well-suited to treating the long-range relaxation at complex surfaces, and allow us to examine a large number of surface planes and terminations at the atomic level. This work extends our previous simulation study of $LiFePO_4$, where we examined its bulk defect and lithium transport properties; we found that Li–Fe anti-site disorder is the lowest energy intrinsic defect, and that dopant incorporation of supervalent cations (*e.g.*, Ti^{4+}, Nb^{5+}) was energetically unfavourable.[24]

Here we report a detailed examination of the energetics and structures of a range of surfaces of $LiFePO_4$, from which crystal morphologies are constructed. Where possible, the results are compared with experimental data including electron micrographs of hydrothermally prepared crystals. The present study forms part of the continuing effort to improve our understanding of the structure–property relationships and, ultimately, the morphological control of $LiFePO_4$ (nano)particles for lithium battery applications.

2. Simulation methods

The simulation techniques used in this study are based upon effective energy minimization procedures modified to treat two-dimensional systems. Such techniques have been used

Department of Chemistry, University of Bath, Bath, UK, BA2 7AY. E-mail: m.s.islam@bath.ac.uk; Fax: +44 (0)1225 386231; Tel: +44 (0)1225 384938

† Electronic supplementary information (ESI) available: Interatomic potential model for bulk and surface calculations, properties of crystal planes and cuts, and notes on surface calculations. See DOI: 10.1039/b715935h

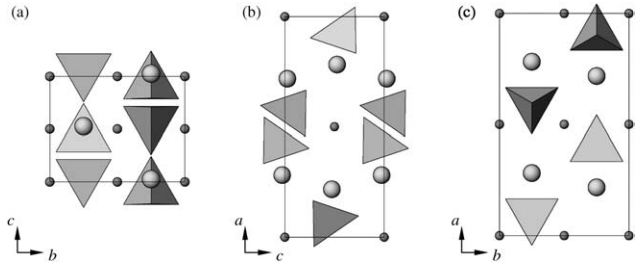

Fig. 1 Unit cell of $LiFePO_4$ viewed down (a) *a* axis, (b) *b* axis, and (c) *c* axis. Li^+: small spheres; Fe^{2+}: large spheres; PO_4^{3-}: tetrahedra (*nb.* ion sizes not to scale).

successfully to examine surfaces of a variety of other binary and ternary oxides.[25,26] Since these methods have been discussed in detail in earlier reviews,[25,26] only the main aspects are outlined here.

The techniques are based on the Born model of ionic solids, with the interactions between pairs of ions described by analytical forms consisting of a long-range Coulombic term plus a short-range term that takes into account both Pauli repulsion and attractive van der Waals interactions. A set of interatomic potential and shell model parameters, developed in our previous study,[24] accurately reproduces the orthorhombic structure of bulk $LiFePO_4$ (space group *Pnma*) (Fig. 1) and these parameters are again used in this study. A three-body term was also included to take account of the angle-dependent nature of the PO_4 tetrahedral units. Similar potential models have been found to work well for compounds such as aluminophosphates[27] and olivine silicates,[28] in which there is a significant degree of covalency.

All the potential parameters used in this study are listed in our earlier paper on bulk defects and dopants in $LiFePO_4$,[24] and are included as supplementary information.† The calculated unit cell parameters using this potential model compare well with neutron diffraction data,[29] as shown in Table 1.

Surface structures and energies of a wide range of low index surfaces of $LiFePO_4$ were calculated using the GULP code.[30] For surface calculations, GULP applies planar 2D periodic boundary conditions to a block of crystal parallel to the plane of interest. The block is split into two regions; atoms of the upper region (region 1) are relaxed explicitly to mechanical equilibrium using efficient minimization algorithms, while those in the lower region (region 2) are held fixed at their equilibrium bulk positions. Region 1 consists of the surface plane and several layers further into the crystal down to region 2. The depths of the surface regions were chosen to be large enough to ensure full relaxation of the surface ions (approximately 200 to 500 ions) and convergence of the surface energy. In this way, the $LiFePO_4$ surfaces are not considered as simple terminations of the bulk lattice. A recent study of nine low index surfaces based on electronic structure methods has also been reported.[31] However, our potential-based methods allow a larger number of particles and surfaces to be treated, ensuring the results are independent of model size, and are thus well suited to these kinds of complex structures.

Table 1 Comparison of calculated and experimental unit cell parameters of $LiFePO_4$

Parameter	Calc./Å	Exp.[29]/Å	Δ/Å
a	10.3713	10.3377	0.0336
b	6.0216	6.0112	0.0104
c	4.6695	4.6950	−0.0255

According to the classification of Tasker,[32] 'as-cut' surfaces can be one of three structural types, which are normally referred to as Types I, II and III. Type I surfaces are formed from layers containing a charge-neutral combination of cations and anions, and thus have no net dipole perpendicular to the surface plane. For Type II surfaces, a finite group of atomic layers parallel to the surface form a charge-neutral, repeated unit with no net dipole normal to the surface normal. For Type III surfaces, by contrast, irrespective of where the crystal is cut (referred to as its "shift"), a dipole moment always exists perpendicular to the surface plane; in this case, convergent surface energies can only be obtained if the surface layer is reconstructed in some way to remove the dipole moment. This usually involves removing a suitable number of ions from one side of the crystal to the other in order to make the crystal slab symmetric about its midpoint.

Once the surface-containing crystal has been constructed, the surface energy, $E_{surface}$, can be calculated both before and after energy minimization according to

$$E_{surface} = \frac{E_S - E_B}{A} \quad (1)$$

where E_S is the energy of the surface-containing region, E_B is the energy of the corresponding number of ions in the bulk crystal, and A is the surface (cross-sectional) area.

Two methods are commonly used to predict the morphology of a crystal from its crystal structure and surface energies. The first is based on the notion, initially expounded by Gibbs,[33] that for a crystal in equilibrium with its surroundings the net surface energy must be minimal for a given volume. This "equilibrium" morphology is obtained by constructing a three-dimensional Wulff plot, in which the distance to the central point {*hkl*} from the origin is taken to be proportional to the surface energy.

The second method for simulating crystal morphologies is based on Hartman–Perdok theory,[34] which attempts to take into account the kinetic factors influencing crystal growth by using the attachment energy of each crystal plane, rather than its equilibrium surface energy. The attachment energy is defined as the energy per formula unit released when a new slice of depth d_{hkl} is attached to the crystal face, and is assumed to be proportional to the growth rate by a layer-by-layer mechanism. Thus surfaces with attachment energies smaller in magnitude will have slower growth rates and be morphologically important. The attachment energy can be expressed as

$$E_{attach} = \frac{E_{crystal} - E_{slice}}{n} \quad (2)$$

where $E_{crystal}$ is the energy of the crystal, E_{slice} is the energy between all the ions within slice *hkl*, and n is the number of formula units per slice. We assume all surfaces form below their critical roughening temperature, and are thus crystallographically flat. A crystal morphology derived by this method is termed the "growth" morphology. (Further details on surface construction and periodic bond chains, as defined by Hartman–Perdok theory, are given as supplementary information.†)

These surface simulation methods have been used to explore crystal morphologies of many inorganic solids,[26,35,36] with the calculated morphologies frequently according well with observation, providing support for the general validity of the methodology.

3. Results and discussion

3.1 Surface structures

$LiFePO_4$ crystallizes in space group *Pnma*, with each orthorhombic unit cell containing four formula units. Each PO_4 tetrahedron is surrounded by four FeO_6 octahedra (three corner-sharing and one edge-sharing), with lithium ions occupying the large open channels running parallel to the *b* axis (Fig. 1). Surface structures and energies were examined for all crystal orientations with indices less than or equal to two, giving a total of nineteen different crystal orientations examined in detail on the atomic level. Phosphate groups were kept intact for all slices to ensure charge neutrality and zero net dipole perpendicular to the surface, and also because breaking up the strongly bonded phosphate tetrahedra would undoubtedly decrease the stability of the surface.

Compared to close-packed binary oxides, $LiFePO_4$ has a relatively low packing efficiency of 68.3%, and this is reflected in the "openness" of the structure, particularly with respect to low index surfaces, which consequently have low 2D area densities. Stable slices can only be formed when all three moieties (Li^+, Fe^{2+} and PO_4^{3+}) are present in stoichiometric ratios, meaning that no Type I surfaces can be formed (as defined in section 2). The disproportionate size of the phosphate unit compared to the other two ions means that all surfaces are necessarily uneven on the atomic scale.

For most Type III surfaces such as (010), the outermost layer initially contained two Li ions, so that the dipole could be cancelled by moving one of these ions to the opposite end of the crystal slab before minimization. The outer layer therefore intrinsically contains 50% Li vacancies relative to the bulk. Generally it was found that surfaces are more stable when the Li vacancies formed by reconstruction are arranged in a zig-zag pattern down the short axis, rather than in a straight or linear configuration. A zig-zag arrangement places the vacancies as far apart as possible within the constraints of the crystal symmetry.

The surface energies, attachment energies and *d*-spacings for the lowest energy crystal slices for each orientation are listed in Table 2. The majority of the surfaces undergo considerable decreases in surface energy, typically 50~80%, resulting in increased stability of the terminating layers even when there is only a small distortion of the surface structure. It is also important to note that the relative order of the surface energies of some crystal orientations changes upon relaxation. This shows the importance of relaxation at the crystal surface, and indicates that the relative surface energies cannot be reliably predicted assuming the crystal to be a rigid, unrelaxed termination of the bulk lattice.

In the majority of cases, the lowest energy termination (usually in terms of both surface energy and attachment energy) is found for Type III surfaces. Only for {110}, {121} and {221} do Type II surfaces have significantly lower energies than their Type III counterparts. This suggests most surfaces will be depleted in Li relative to the bulk lattice, even in the fully lithiated $LiFePO_4$ compound.

Table 2 Calculated properties of low index surfaces of $LiFePO_4$

Plane	Tasker surface type	*d*-spacing, d_{hkl}/Å	Surface energy, $E_{surface}$/J m^{-2}		Attachment energy, E_{attach}/J m^{-2}
			Unrelaxed	Relaxed	
(001)	III	2.33	2.40	1.11	−11.18
(010)	III	3.01	1.64	0.72	−5.74
(100)	III	5.19	2.12	0.87	−3.39
(011)	III	3.69	2.55	0.75	−6.43
(012)	II	1.09	4.50	1.02	−27.31
(021)	II	1.27	2.41	0.82	−18.03
(101)	III	4.26	1.65	0.88	−3.42
(102)	II	2.28	3.29	1.15	−19.85
(110)	II	2.60	3.62	0.92	−16.25
(111)	III	3.48	2.94	0.89	−5.34
(112)	III	2.13	2.57	0.88	−16.81
(120)	III	1.45	3.53	0.86	−17.43
(121)	II	2.46	2.44	0.94	−11.27
(122)	III	1.82	2.65	0.80	−14.17
(201)	III	3.47	1.37	0.71	−4.27
(210)	III	3.93	2.61	0.90	−5.55
(211)	III	3.01	2.51	0.80	−8.60
(212)	III	2.01	2.26	0.86	−11.60
(221)	II	2.27	2.52	0.79	−10.69

The lowest surface energies in Table 2 are found for (010), (011) and (201) surfaces, whereas the lowest attachment energies are found for (010), (100), (101) and (201). The low energy (010), (100), (101) and (201) surfaces are presented in more detail in Fig. 2–4 by way of example. In each case the terminating layer contains all three moieties (Li, Fe and PO_4).

The (010) surface is of particular interest because it lies normal to the direction of the most facile pathway for Li^+ conduction[24,37] (Fig. 2). Our previous simulation study[24] found that Li ion transport is one-dimensional along the [010] channel, with the Li ions following a non-linear curved trajectory between adjacent Li sites. Although blocking electrode measurements over a narrow temperature range by Amin *et al.*[38] found that lithium ion diffusion in single crystals of $LiFePO_4$ appears to be two-dimensional, this is not consistent with the above-mentioned theoretical calculations,[24,37] or indeed the strongly anisotropic nature of

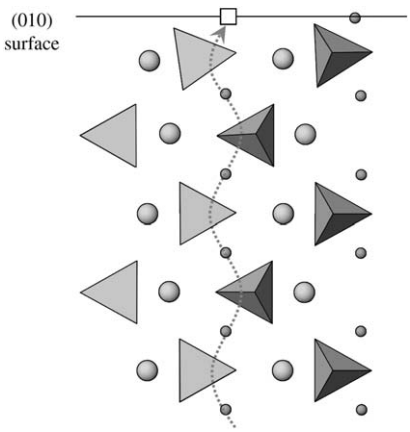

Fig. 2 Side view of the relaxed (010) surface, showing tilting of the PO_4 tetrahedron near the Li^+ vacancy (open square) in the topmost layer. The sinusoidal Li^+ migration path (dotted line) identified from previous work[24] lies normal to the surface plane. Li^+: small spheres; Fe^{2+}: large spheres.

the orthorhombic structure. It is worth noting that tracer diffusion studies of olivine-structured Fe_2SiO_4 found Fe ion transport to be anisotropic.[39]

The low surface and attachment energies obtained suggest (010) will be prominent in the crystal morphology, which may help expedite the reversible Li^+ intercalation process. The (010) surface is also important in relation to studies of the $LiFePO_4$–$FePO_4$ two-phase boundary interface; for example, high-resolution electron energy loss spectroscopy by Laffont *et al.*[40] revealed that the phase transition occurs by successive emptying (or filling) of the Li^+ channels along the b_{Pnma} axis, while TEM studies by Chen *et al.*[41] found that phase separation occurs along the b_{Pnma} direction with fully lithiated $LiFePO_4$ forming on (010) surfaces.

The relaxed (010) structure, which is Li^+ deficient in the terminating layer, is illustrated from different viewpoints in Fig. 2 (side) and 3 (above), and like most other surfaces examined has an uneven topology. The low density of the structure, in which the oxygen sublattice is not densely packed, means that no significant rumpling occurs; the simulations find only a small rotation or twisting of the phosphate tetrahedron neighbouring the Li vacancy. The outermost Li ion displaces the most, moving towards the neighbouring phosphate group (Fig. 3). Furthermore, this Li^+ ion is three-coordinated, compared to six-fold coordination in the bulk, with the Li–O bond lengths contracted by 0.1–0.15 Å. The Fe ions in the top layer, which are not as exposed as the Li ions, have their coordination reduced from six to five, with little change in the Fe–O bond lengths.

Fig. 3 shows the simulated upper layers of the (010) surface viewed from above, with the Li channels visible between phosphate tetrahedra. Li transfer between the electrode and electrolyte in a lithium battery should be optimal through this surface because the channels are perpendicular to the terminating plane, with the Li ions presented with the widest "diffusion window" through which to leave/enter the structure.

The structures of (100), (101) and (201) surfaces in Fig. 4 contain the same components (Li^+, Fe^{2+} and PO_4^{3-} moieties) as the (010) surface, also with 50% Li vacancies in the top layer, but these are arranged in very different ways, resulting in structurally distinct surface topologies. Although the calculated energies

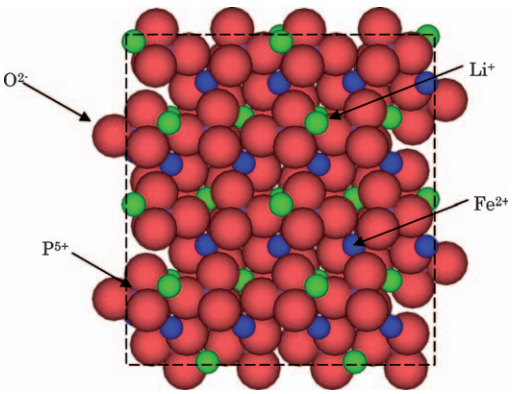

Fig. 3 Topmost two layers of the (010) surface viewed from above, showing zigzag arrangement of outermost Li^+ ions. Li^+: green; Fe^{2+}: blue; P^{5+}: purple; O^{2-}: red. The small phosphorus ions lie enclosed at the centres of the oxygen tetrahedra.

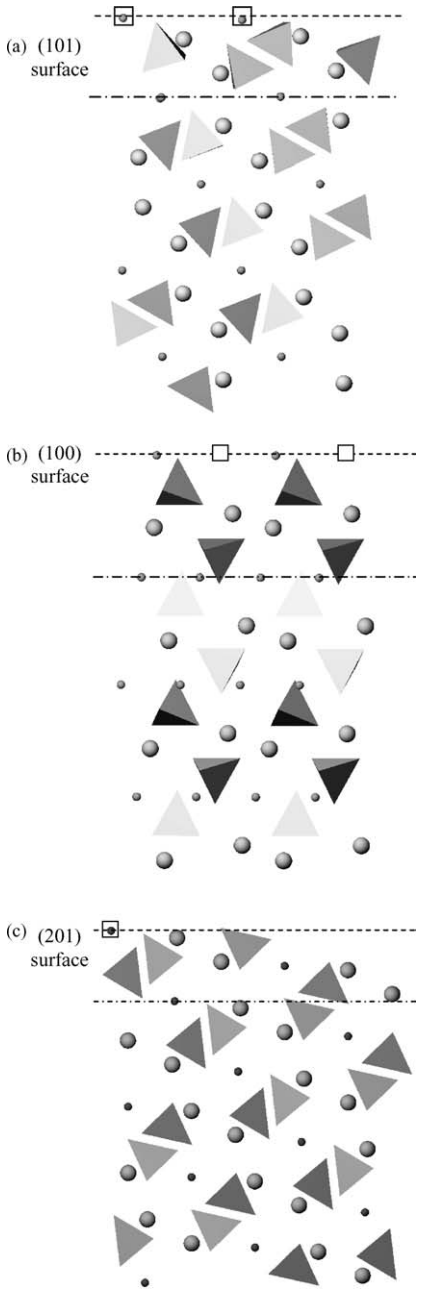

Fig. 4 Side views of relaxed (a) (101), (b) (100), and (c) (201) surfaces of $LiFePO_4$. In (a) and (c) Li ions and Li vacancies alternate into the page. Some tilting of the phosphate groups in the surface layers is evident for (101). Li^+: small spheres; Fe^{2+}: large spheres; open squares: Li vacancies. Growth slices are demarcated by dotted-dashed lines.

are similar, the alignments of the different moieties, particularly the Li ions, will likely result in very different insertion and extraction characteristics for these surfaces compared with (010).

3.2 Calculated and experimental crystal morphologies

As with most materials, direct comparison of surface energies with experiment is not possible for $LiFePO_4$ because of the lack of corresponding data. Nevertheless, the crystal morphology is one indirect measure which can be predicted from the surface and attachment energies (using the methods outlined in

section 2) that can be compared with crystalline (nano)particles observed by electron microscopy. The simulation approach has been applied successfully to the prediction of crystal morphologies of a wide variety of solids such as calcite,[26] apatite phosphates,[35] anatase TiO_2,[36] and La_2NiO_4.[42]

Fig. 5 (a) shows the equilibrium crystal morphology calculated using the lowest surface energies after energy minimization. After relaxation, the range of surface energies narrows significantly, so that most surfaces have similarly low energies. This can be rationalised as being a result of the topology and ionic moieties at the surfaces being very similar. Consequently, the equilibrium morphology takes on a more rounded, isometric appearance, with {010}, {201}, {011}, and {100} faces prominent (in the absence of water, additives or coating layers). For nano-sized or smaller crystals, where rearrangement of the crystal at each stage of the growth is possible, a morphology close to the equilibrium form might be expected.

Fig. 5 (b) shows the calculated growth morphology, which is terminated by {010}, {100} and {101} faces. These dominant faces are expected to play a significant role in the electrochemical and surface exchange properties of the material. The crystal shape is anisotropic, with an elongated hexagonal prism-like habit capped by {010} faces; this morphology is similar to SEM images by Franger *et al.*,[15] illustrated in Fig. 6.

A range of synthesis techniques and conditions have been used to prepare $LiFePO_4$ experimentally, producing a variety of particle morphologies and size distributions as reported in the literature. For example, crystallites have been observed in the shape of hexagonal- or diamond-type platelets,[14,20] rectangular prisms,[20] rods and block shapes;[15] some of these are represented schematically in Fig. 6. The precise surface planes are not easily assigned from experiment, however, particularly given the small

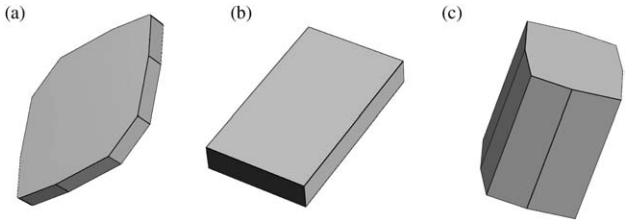

Fig. 6 Schematic diagrams of observed crystal morphologies of $LiFePO_4$ produced under different experimental conditions; (a) hexagonal platelet,[14,20] (b) rectangular prism,[14] and (c) block-shape.[15]

sizes of the particles in crystallite agglomerates, and atomic level detail is difficult to obtain.

Chen *et al.*[20] have investigated the $LiFePO_4$ to $FePO_4$ phase transition in hydrothermally grown hexagonal "plate-like" crystals using electron microscopy. Their TEM analysis[20] revealed the large faces of these particles to lie normal to the *b* axis, with the long axis parallel to *c*. Ellis *et al.*[14] have also produced uniformly "diamond-shaped" and plate-like prismatic particles by hydrothermal solution, and X-ray diffraction also found the larger particles to be dominated by the (010) surface. By varying the concentration of the solvent and synthesis temperature, however, they were able to prepare particles varying in size from nanometres to microns. In the well-defined particles, {010} surfaces constitute roughly 80% of a particle's surface area.

Fig. 7 shows our reproduction of the plate-like morphology, which is directly compared with SEM images of crystallites prepared hyrdothermally as described by Chen *et al.*[20] According to our morphology, in order for the {010} surfaces to dominate, the attachment energy (or surface energy in the case of particles at equilibrium) of the {010} layers must be at least three times

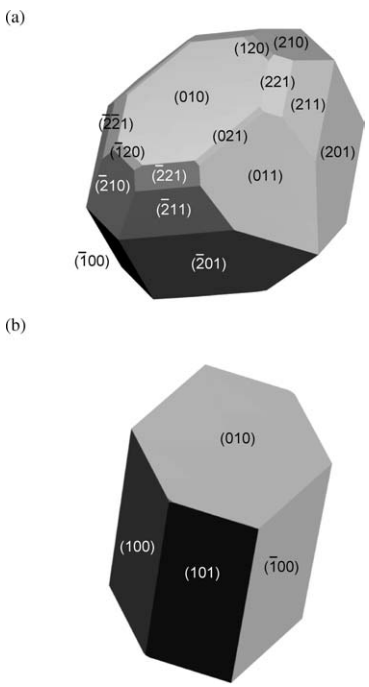

Fig. 5 Theoretical crystal morphologies of $LiFePO_4$; (a) equilibrium morphology from relaxed surface energies, and (b) growth morphology from attachment energies.

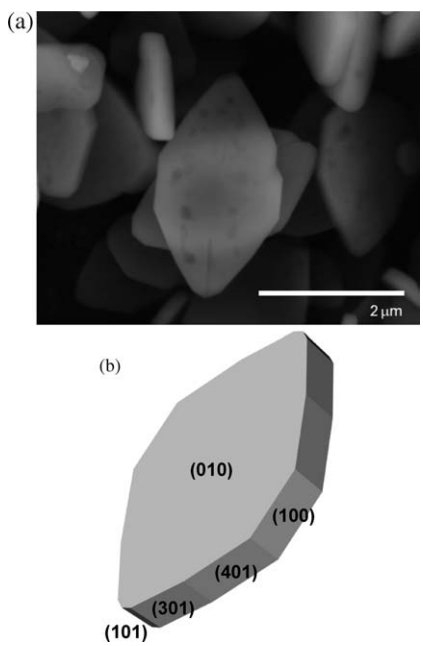

Fig. 7 Calculated and experimental plate-like morphologies of $LiFePO_4$. (a) SEM micrograph of non-coated $LiFePO_4$ crystallites from hydrothermal synthesis; (b) simulated morphology obtained using faces identified from TEM.[43]

smaller than that of the next most stable surface, {100}. The exposure of the (010) surface is important, since as already noted (Fig. 2), it is normal to the most facile pathway for lithium ion migration,[24] and hence electrochemically active. The thinness of the plate-like morphologies in the [010] direction should reduce the transport path length of lithium ions, and thus may enhance the rate capability of a cathode prepared from such a material.

As the (010) surface is perpendicular to the direction of diffusion of the Li ions, it is likely that the lithium content at the surface (through intercalation and de-intercalation) has a powerful influence on the surface energies, and hence morphology; this necessarily involves the change in charge state and electronic density of the Fe ions from Fe^{2+} to Fe^{3+} and *vice versa*. As discussed by Woensdregt,[34] the charge state at the surface can have a profound effect on the energies of the faces, and hence the overall crystal morphology.

In practice, the growth rate is also controlled by many external factors, such as temperature, solvent effects, and molecules adsorbed at the surface. This explains the wide variety of morphologies observed experimentally, and warrants further investigation. Indeed, one of the aims of this study is to encourage further work in this area using surface sensitive techniques. Effects of water adsorption constitute a substantial and complex investigation for the large number of surface planes we have modelled; this is currently work in progress.

4. Conclusions

Advanced simulation techniques have been used to provide atomic-scale detail of the surface structures and crystal morphologies of the $LiFePO_4$ lithium battery material, which are relevant to its electrochemical behaviour. Where possible, the results were compared with electron microscopy images of experimentally prepared crystals. The main points can be summarized as follows:

(1) Relaxed surface structures and energies were calculated for 19 low index planes of $LiFePO_4$. The surface structures exhibit a complex, uneven topology on account of the different sizes of the three constituent moieties, Li^+, Fe^{2+} and PO_4^{3-}. The majority of the surfaces undergo considerable relaxation, which confirms that the surface chemistry and electrochemical activity cannot be reliably predicted by assuming rigid, unrelaxed terminations of the bulk lattice.

(2) The calculated equilibrium morphology of $LiFePO_4$ takes on a rounded, isometric appearance, with {010}, {201}, {011}, and {100} faces prominent. Almost all of the low energy surfaces are lithium-deficient relative to the bulk lattice, requiring Li vacancies at the surface; this may become increasingly important for Li intercalation with decreasing size of the crystalline particles.

(3) The calculated growth morphology is terminated by {010}, {100} and {101} faces, which are expected to play a significant role in the electrochemical properties of the material. The crystal shape is anisotropic, with an elongated hexagonal prism-like shape capped by {010} faces; this morphology is consistent with some SEM images of pure $LiFePO_4$, although different synthesis routes have produced a variety of crystallite morphologies such as hexagonal-type platelets, rectangular prisms and block-type shapes.

(4) The (010) surface is prominent in both calculated equilibrium and growth morphologies. The exposure of the (010) surface is significant since it is normal to the most facile pathway for lithium ion conduction (along the [010] channel), and hence important for the reversible insertion/de-insertion of lithium ions. The (010) surface may also be important in relation to studies of the $LiFePO_4$–$FePO_4$ boundary interface and warrants further investigation.

(5) SEM images of plate-like crystallites of uncoated $LiFePO_4$ from hydrothermal synthesis exhibiting large (010) faces have been reproduced by our methods for direct comparison. The thinness of the plate-like morphologies parallel to the b_{Pnma} axis requires the (010) surface to be significantly lower in energy than the other surfaces. This reduction in diffusion path length of lithium ions is expected to enhance the electrochemical performance of a cathode prepared from such a material.

Acknowledgements

We thank the EPSRC for funding as part of the Supergen Energy Storage Consortium (grant code EP/D031672/1), and Prof. Julian Gale at Curtin University, Australia, for providing GULP. We are also grateful to Dr Tom Richardson and Dr Guoying Chen at Lawrence Berkeley National Laboratory, USA, for useful discussions and providing microscopy data.

References

1 A. S. Aricò, P. G. Bruce, B. Scrosati, J.-M. Tarascon and W. van Schalkwijk, *Nat. Mater.*, 2005, **4**, 366; M. M. Thackeray, S.-H. Kang, C. S. Johnson, J. T. Vaughey, R. Benedek and S. A. Hackney, *J. Mater. Chem.*, 2007, **17**, 2069; M. S. Whittingham, Y. Song, S. Lutta, P. Y. Zavalij and N. A. Chernova, *J. Mater. Chem.*, 2005, **15**, 3362; A. K. Padhi, K. S. Nanjundaswamy, C. Masquelier and J. B. Goodenough, *J. Electrochem. Soc.*, 1997, **144**, 2581.
2 A. K. Padhi, K. S. Nanjundaswamy and J. B. Goodenough, *J. Electrochem. Soc.*, 1997, **144**, 1188.
3 R. Dominko, M. Bele, J. M. Goupil, M. Gaberseek, D. Hanzel, I. Arcon and J. Jamnik, *Chem. Mater.*, 2007, **19**, 2960.
4 Y. Wang, J. Wang, J. Yang and Y. Nuli, *Adv. Funct. Mater.*, 2006, **16**, 2135.
5 C. R. Sides, F. Croce, V. Y. Young, C. R. Martin and B. Scrosati, *Electrochem. Solid-State Lett.*, 2005, **8**, A484.
6 K. Zaghib, A. Mauger, J. B. Goodenough, F. Gendron and C. M. Julien, *Chem. Mater.*, 2007, **19**, 3740.
7 B. Ellis, L. K. Perry, D. H. Ryan and L. F. Nazar, *J. Am. Chem. Soc.*, 2006, **128**, 11416.
8 N. Ravet, Y. Chouinard, J. F. Magnan, S. Besner, M. Gauthier and M. Armand, *J. Power Sources*, 2001, **97–8**, 503.
9 K. F. Hsu, S. Y. Tsay and B. J. Hwang, *J. Mater. Chem.*, 2004, **14**, 2690; J. Barker, M. Y. Saidi and J. L. Swoyer, *Electrochem. Solid-State Lett.*, 2003, **6**, A53.
10 R. Dominko, M. Gaberscek, J. Drofenik, M. Bele, S. Pejovnik and J. Jamnik, *J. Power Sources*, 2003, **119**, 770.
11 H. Gabrisch, J. D. Wilcox and M. M. Doeff, *Electrochem. Solid-State Lett.*, 2006, **9**, A360.
12 P. Subramanya Herle, B. Ellis, N. Coombs and L. F. Nazar, *Nat. Mater.*, 2004, **3**, 147.
13 S.-Y. Chung, J. T. Bloking and Y.-M. Chiang, *Nat. Mater.*, 2002, **1**, 123.
14 B. Ellis, H. K. Wang, W. R. M. Makahnouk and L. F. Nazar, *J. Mater. Chem.*, 2007, **17**, 3248.
15 S. Franger, F. Le Cras, C. Bourbon and H. Rouault, *J. Power Sources*, 2003, **119–121**, 252; S. Franger, F. Le Cras, C. Bourbon, C. Benoit, P. Soudan and J. Santos-Peña, *Recent Res. Devel. Electrochem.*, 2005, **8**, 225.

16 B. Ellis, P. Subramanya Herle, Y.-H. Rho, L. F. Nazar, R. Dunlap, L. K. Perry and D. H. Ryan, *Faraday Discuss.*, 2006, **134**, 1.
17 D.-H. Kim and J. Kim, *Electrochem. Solid-State Lett.*, 2006, **9**, A439.
18 C. Delacourt, P. Poizot, S. Levasseur and C. Masquelier, *Electrochem. Solid-State Lett.*, 2006, **9**, A352.
19 N. Meethong, H.-Y. S. Huang, S. A. Speakman, W. C. Carter and Y.-M. Chiang, *Adv. Funct. Mater.*, 2007, **17**, 1115.
20 G. Chen, X. Song and T. J. Richardson, *Electrochem. Solid-State Lett.*, 2006, **9**, A295.
21 S. Yang, Y. Song, P. Y. Zavalij and M. S. Whittingham, *Electrochem. Commun.*, 2002, **4**, 239.
22 Y.-H. Rho, L. F. Nazar, L. Perry and D. Ryan, *J. Electrochem. Soc.*, 2007, **154**, A283.
23 O. Haas, A. Deb, E. J. Cairns and A. Wokaun, *J. Electrochem. Soc.*, 2005, **152**, A191.
24 M. S. Islam, D. J. Driscoll, C. A. J. Fisher and P. R. Slater, *Chem. Mater.*, 2005, **17**, 5085.
25 J. H. Harding, in *Computer Modelling in Inorganic Crystallography*, ed. C. R. A. Catlow, Academic Press, San Diego, 1997, ch. 7, pp. 185–199.
26 S. C. Parker, N. H. de Leeuw and S. E. Redfern, *Faraday Discuss.*, 1999, **114**, 381.
27 N. J. Henson, A. Cheetham and J. D. Gale, *Chem. Mater.*, 1996, **8**, 664.
28 A. M. Walker, K. Wright and B. Slater, *Phys. Chem. Miner.*, 2003, **30**, 536.
29 G. Rousse, J. Rodriguez-Carvajal, S. Patoux and C. Masquelier, *Chem. Mater.*, 2003, **15**, 4082.
30 J. D. Gale and A. L. Rohl, *Mol. Simul.*, 2003, **29**, 291.
31 L. Wang, F. Zhou, Y. S. Meng and G. Ceder, *Phys. Rev. B*, 2007, **76**, 165435.
32 P. W. Tasker, *J. Phys. C: Solid State Phys.*, 1979, **12**, 4977.
33 J. W. Gibbs, *Collected Works*. Longman, New York, 1928.
34 C. F. Woensdregt, *Faraday Discuss.*, 1993, **95**, 97.
35 D. Mkhonto and N. H. de Leeuw, *J. Mater. Chem.*, 2002, **12**, 2633.
36 C. L. Olson, J. Nelson and M. S. Islam, *J. Phys. Chem. B*, 2006, **110**, 9995.
37 D. Morgan, A. Van der Ven and G. Ceder, *Electrochem. Solid-State Lett.*, 2004, **7**, A30; C. Ouyang, S. Shi, Z. Wang, X. Huang and L. Chen, *Phys. Rev. B*, 2004, **69**, 104303.
38 R. Amin, P. Balaya and J. Maier, *Electrochem. Solid-State Lett.*, 2004, **10**, A13.
39 S. Aggarwal, J. Töpfer, T.-L. Tsai and R. Dieckmann, *Solid State Ionics*, 1997, **101–103**, 321; K. Ullrich and K. D. Becker, *Solid State Ionics*, 2001, **141–142**, 307.
40 L. Laffont, C. Delacourt, P. Gibot, M. Y. Wu, P. Kooyman, C. Masquelier and J.-M. Tarascon, *Chem. Mater.*, 2006, **18**, 5520.
41 G. Chen, X. Song and T. J. Richardson, *J. Electrochem. Soc.*, 2007, **154**, A627.
42 M. S. D. Read, M. S. Islam, G. W. Watson and F. E. Hancock, *J. Mater. Chem.*, 2001, **11**, 2597.
43 G. Chen and T. J. Richardson, personal communication.

Journal of Materials Chemistry

www.rsc.org/materials

Volume 18 | Number 11 | 21 March 2008 | Pages 1161–1268

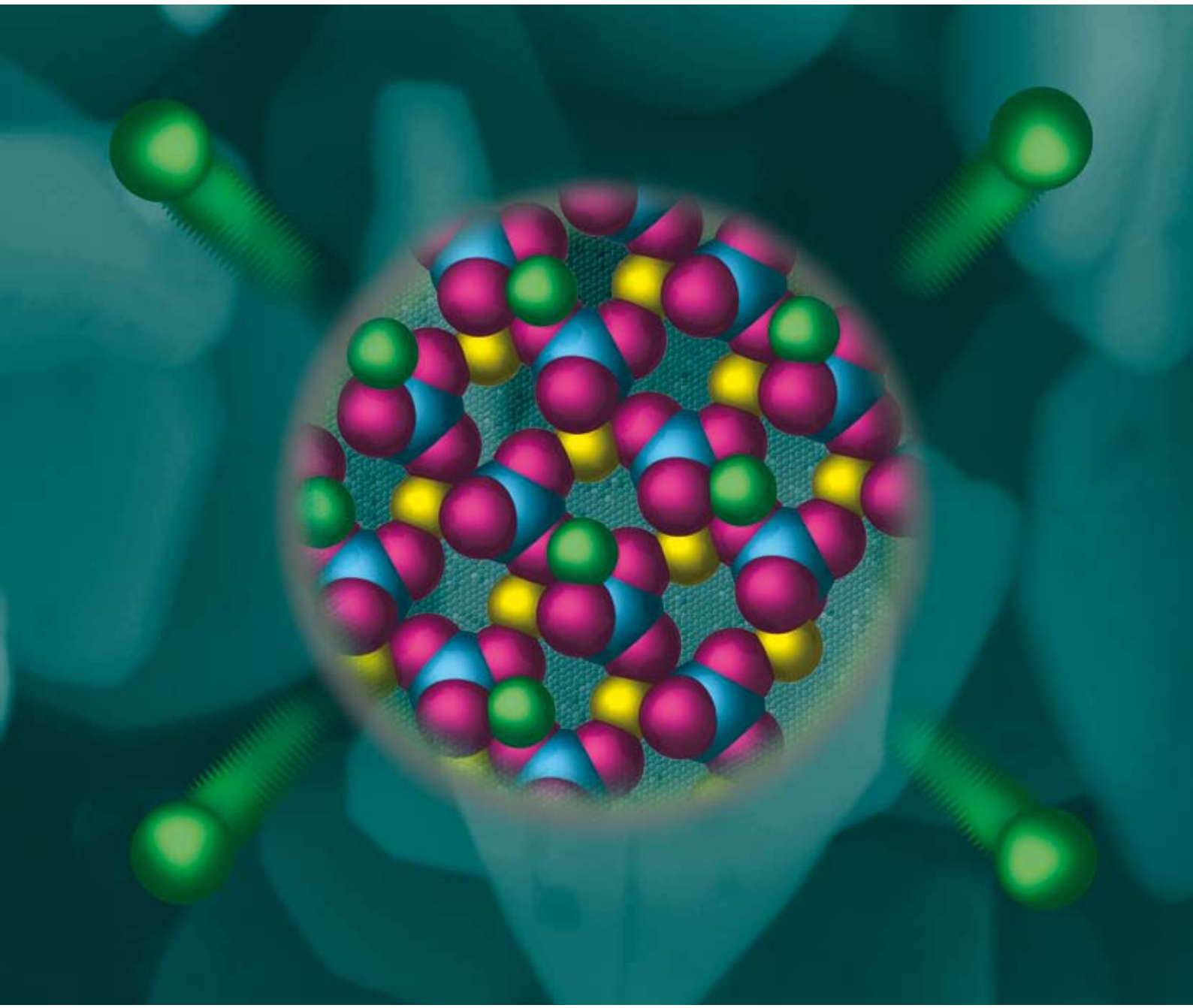

ISSN 0959-9428

RSC Publishing

0959-9428(2008)18:11;1-1